Journal of Hydrology 615 (2022) 128692

Contents lists available at ScienceDirect

Journal of Hydrology

journal homepage: www.elsevier.com/locate/jhydrol

Research papers

Random-walk-path solution of unsteady flow equations for general channel networks

Hongwu Tang [a,b], Xiao Luo [a], Saiyu Yuan [a,b,*], Yang Xiao [a,b], Dongfang Liang [c], Carlo Gualtieri [d]

[a] State Key Laboratory of Hydrology-Water Resources and Hydraulic Engineering, Hohai University, Nanjing 210024, China
[b] Yangtze Institute for Conservation and Development, Nanjing 210024, China
[c] Department of Engineering, University of Cambridge, Cambridge CB2 1PZ, UK
[d] Department of Structures for Engineering and Architecture, University of Napoli Federico II, Napoli, Italy

ARTICLE INFO

Editor: Corrado Corradini
Associate Editor: Philip Brunner.

Keywords:
Random walk path
Unsteady flow
Saint-Venant equations
Open Channel
Channel networks

ABSTRACT

The random walk path method (RWP) is a stochastic model that transforms the solution of the unsteady open channel flow equations into a probability problem. In this paper, this method is introduced to solve the discretized Saint-Venant equations, with probabilistic representation of the water levels at junctions. Different boundary conditions, which specify either water levels or discharge hydrographs, can be implemented by specifying how walkers react when arriving at the boundaries. The pointwise solution at river junctions can be obtained via random walk simulations. The efficacy of the model was verified against the following test cases: (1) a real-world looped channel example documented in the manual of the software Hec-Ras and (2) a hypothetical channel system consisting of dendritic and divergent networks. The number of random simulations is an important aspect of the RWP method and needs to be chosen by considering the trade-off between precision and computational efficiency. The impact of the boundary water level or discharge on the water levels at internal nodes can be quantitatively evaluated by adopting the terminal weights, which present a distinct advantage of the RWP method. This assessment of water levels can serve as a guide in the operation of hydraulic controls, such as dams, sluices and pumps, to effectively regulate the flow in mitigating flood risks.

1. Introduction

Modelling of unsteady flow in open channel networks plays an important role in many hydraulic applications, such as flood forecasting (Bates and De Roo, 2000; Beltaos et al., 2012; Nazari and Seo, 2021), drainage system design (Henine et al., 2014), irrigation (Assar et al., 2020), algae control (Fovet et al., 2013) and wastewater management (Akella and Bhallamudi, 2019). Numerical simulation is extensively used to study the hydrodynamic processes in channel networks, by solving the one-dimensional flow equations, commonly known as the Saint–Venant equations. These equations (Cunge et al., 1980) are a set of non-linear partial derivative equations which are difficult to solve analytically. Numerical techniques are widely used in the discretization of the Saint-Venant equations to obtain non-linear algebraic equations. Finite difference schemes (El Kadi Abderrezzak and Paquier, 2009; Qi et al., 2022; Sen and Garg, 2002) are the most commonly applied techniques due to their advantages, such as a small amount of computation and ease of implementation. In the past two decades, the finite volume method (Hodges, 2019; Kesserwani et al., 2008a; Sarkhosh et al., 2020) was widely applied to solve the Saint-Venant equations, limited mostly to 2D cases (Liang et al., 2007; Zhao et al., 2019). The non-linear equations are solved using iterative techniques such as the Newton-Raphson method (Janicke and Kost, 1998; Zhu et al., 2011) or through linearization. For modelling the flow in a single channel, the coefficient matrix of the linear equation system is banded, and efficient methods such as the double sweep algorithm can be used to solve the well-structured matrix equation (Cunge et al., 1980). However, for a channel network, the coefficient matrix does not exhibit the banded property due to difficulties in generating a coefficient matrix of the minimum bandwidth considering the role of junctions. Directly solving these coefficient matrices usually requires considerable computational time and computer storage.

Some attempts have been made in the past to simplify these complicated or extremely large coefficient matrices, with the initial research focused on dendritic channel networks. The separate-segment method (Akan and Yen, 1981; Fread, 1973) was used to split the

* Corresponding author at: State Key Laboratory of Hydrology-Water Resources and Hydraulic Engineering, Hohai University, Nanjing 210024, China.
E-mail address: yuansaiyu@hhu.edu.cn (S. Yuan).

https://doi.org/10.1016/j.jhydrol.2022.128692
Received 22 August 2022; Received in revised form 12 October 2022; Accepted 20 October 2022
Available online 9 November 2022

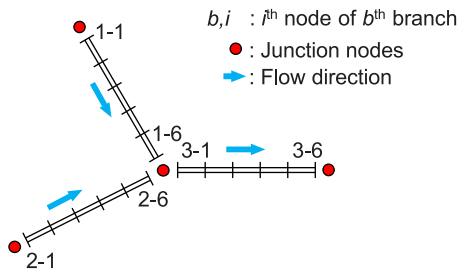

Fig. 1. A typical junction scheme with three branches.

channels network into overlapping and independent components for computation. However, it needed a large number of iterations and failed to accurately describe the physical phenomena near channel junctions. Some scholars transformed the matrix into formats that were suitable for the double scan algorithm techniques such as matrix diagonalization or recursive equations (Choi and Molinas, 1993). In addition, specific node numbering was used to obtain banded matrices with reduced bandwidth (Nguyen and Kawano, 1995). Thus, all the above algorithms have very specific requirements regarding the topology or node numbering of the channel network and cannot be applied easily to networks containing loops.

The three-step algorithm is a generalized algorithm for unsteady flow modelling which is suitable for any type of channel network (Fang et al., 2012; Sen and Garg, 2002; Sen and Garg, 1998; Zhang and Shen, 2007). This algorithm splits the channel network into segments. The end-node variables of each channel are calculated first, followed by the solution for variables at all other sections by a backward substitution. This method improves the computational efficiency by reducing the order of the computational matrix. However, the entire set of equations needs to be solved simultaneously and thus the advantage of the banded nature is lost (Zhu et al., 2011). Another problem with the three-step algorithm is that it is difficult to explicitly check the individual contributions of model components in the absence of additional tools for sensitivity analysis.

The random walk path method (RWP) is a method 0f solving mathematical problems via random walk simulations. The basic idea of the RWP method is to establish a random walk process whose parameters are linked to the solution of the equation. The statistical characteristics of the parameters, which yield the exact value of the solution, can be obtained through sampling experiments. There are distinctions between this method and the particle tracking method, which is a typical mesh-free approach for modelling contaminant transport (Roubinet et al., 2010; Yang and Liang, 2020). Although both methods are based on random motions of particles, they are different in terms of the mathematical bases. The particle tracking method is based on Fokker–Planck equation (LaBolle et al., 1996) and is known as one of the Lagrangian methods, while the RWP method is an application of the Feynman-Kac theorem. Nan and Wu (2018) gave a detailed description of these two methods from a theoretical point of view. To avoid confusion, the method adopted in this paper is termed the RWP method. For problems that are too complex to get an analytical solution, or have no analytical solution, the RWP method is an effective way to find a numerical solution. This approach provides a new perspective for the solution of partial differential equations (PDEs). Different schemes of the RWP method have been developed in the past and applied to solve PDEs of various physical processes (Maire and Nguyen, 2016; Mascagni and Simonov, 2004; Simonov and Mascagni, 2004). In addition, the RWP method can be used to calculate the interdependence between nodes in a network, known as the correlation. Specifically, with regard to hydraulics, RWP has been successfully applied for solving PDEs of complicated groundwater problems and pumping well management (Nan et al., 2020; Nan and Wu, 2018). Solving steady-state problems in channel networks using the RWP method has also been well studied (Chen et al., 2001). Wang et al. (2016) made an attempt to apply it to unsteady flow modelling, but the consistency between the mathematical expectation of probabilistic representation and the deterministic solution was not well proven; moreover, only looped networks were considered and the boundary condition was restricted to the water-level-hydrograph.

This present study focuses on the RWP method applied to unsteady flow modelling of channel networks and its potential prospects in water conservancy projects management. A probabilistic description of the solutions to the discretized Saint-Venant equations is presented and its mathematical expectation has been derived. This paper also presents the conditions under which they are applicable by taking into account the limitations of the transition probability. The key to dealing with different boundary conditions, such as water-level-hydrograph and discharge-hydrograph, is to define the reaction of the walkers when they meet the boundaries.

2. Methodology

2.1. Basic equations and formulation of the problem

The Saint-Venant equations for open channel flows can be expressed as follows.

$$\begin{cases} \dfrac{\partial Q}{\partial x} + L_t \dfrac{\partial Z}{\partial t} = 0 \\ \dfrac{\partial Q}{\partial t} + \dfrac{\partial QV}{\partial x} + gA\left(\dfrac{\partial Z}{\partial x} + J\right) = 0 \end{cases} \tag{1}$$

where Q [m^3/s] is the volumetric discharge; L_t [m] is the river width; Z [m] is the water level; t [s] is time; V [$m\,s^{-1}$] is the velocity; A [m^2] is the flow area of cross–section; $g = 9.81\ m\ s^{-2}$ is the gravitational acceleration; and J [$-$] is the friction slope. Along a channel, J can be expressed as $J = Q|Q|/D^2$, where D [$m^6 s^{-2}$] is the conveyance function.

Among the numerous numerical schemes for solving the Saint-Venant equations, the implicit scheme has the advantage of allowing for large time steps (Zhu and Chen, 2019 and references therein). In this paper, Eq. (1) is discretized using the four-point implicit Preissmann scheme which exhibits good numerical stability (Sen and Garg, 2002). This scheme results in a system of nonlinear algebraic equations between cross-sections i and j for each small river section, which can be expressed as follows:

$$\begin{cases} as_{1,i+1}Q_i + bs_{1,i+1}Z_i = cs_{1,i+1}Q_{i+1} + ds_{1,i+1}Z_{i+1} + es_{1,i+1} \\ as_{2,i+1}Q_i + bs_{2,i+1}Z_i = cs_{2,i+1}Q_{i+1} + ds_{2,i+1}Z_{i+1} + es_{2,i+1} \end{cases} \tag{2}$$

where Z_i, Z_{i+1}, Q_i and Q_{i+1} are the water levels and discharges at cross-sections i and $i+1$, respectively; as_1, bs_1, cs_1, ds_1, es_1, as_2, bs_2, cs_2, ds_2, and es_2 are the coefficients of the discretized Saint-Venant equations (see Appendix A), and subscript $i+1$ is omitted here, for the sake of brevity.

The forward elimination in the three-step method (Sen and Garg, 2002) is used here to derive the basic simultaneous equations. For a branch involving N_c number of cross-section, $2N_c$-2 number of coupled equations can be established according to Eq. (2). The number of unknown variables is $2N_c$, so the equations can be solved if we know two of the variables. For each branch, the variables corresponding to the interior cross-sections are not directly connected to those corresponding to other branches. Therefore, the end-node variables of all the branches can be separated to establish global branch equations. The $2N_c$-2 equations for a branch can be reduced to two equations involving four variables at the two ends of the branch ($Z_{b,1}$, Z_{b,i_e}, $Q_{b,1}$ and Q_{b,i_e}). This can be achieved using the chasing method (Zhang and Shen, 2007). In other words, the discharge at the first and last sections of a branch can be expressed as linear functions of the water levels as follows:

$$\begin{cases} Q_{b,1} = \alpha_b + \beta_b Z_{b,1} + \zeta_b Z_{b,i_e} \\ Q_{b,i_e} = \varepsilon_b + \eta_b Z_{b,i_e} + \gamma_b Z_{b,1} \end{cases} \tag{3}$$

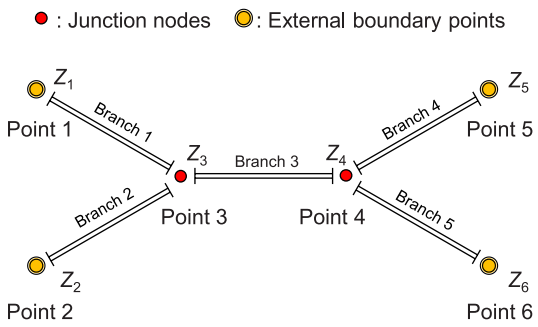

Fig. 2. A typical channel network with four boundaries.

Table 1
The boundary cross-section and types of boundary conditions involved in this study.

	Types of boundary conditions	
	discharge-hydrograph	water-level-hydrograph
Test case 1		C17, C1
Test case 2	C17	C1
Test case 3		4–1, 5–1, 8–1, 3–6, 10–11

Table 2
RMSE and MAPE for simulated water level in looped river network.

	$N_{RS} = 5$		$N_{RS} = 50$		$N_{RS} = 100$	
Time	RMSE (m)	MAPE	RMSE (m)	MAPE	RMSE (m)	MAPE
$t = 3$ h	0.0095	0.134%	0.0091	0.117%	0.0064	0.083%
$t = 6$ h	0.0068	0.097%	0.0064	0.069%	0.0070	0.095%
$t = 9$ h	0.0125	0.158%	0.0044	0.064%	0.0070	0.096%
$t = 12$ h	0.0105	0.130%	0.0039	0.056%	0.0029	0.040%
$t = 24$ h	0.0061	0.088%	0.0077	0.103%	0.0039	0.055%

Table 3
Channel characteristics for network-2.

Channel number	Length (m)	Bed width (m)	Side slope	Bed slope	Manning's n (s $m^{-1/3}$)	Number of reaches
1,10	2000	100	1:2	0.0001	0.025	10
2,4,5,7,8	1000	50	1:2	0.0002	0.025	5
3,6,9	1000	75	1:2	0.0001	0.025	5

Table 4
Computational costs (unit: millisecond). Note that all the numbers listed here exclude the time of post-processing and values in brackets indicate the time of equation solving.

Index	Simulation setup	Hec-Ras	Traditional three-step method	RWP		
				N_{RS} = 5	N_{RS} = 50	N_{RS} = 100
S1	Case 1-Δt = 60s	~2000	1132.8(44)	1128.2 (45)	1173 (65)	1205.6 (100)
S2	Case 2-Δt = 60s	~2000	1132.8(44)	1153 (34)	1200 (68)	1231 (139)
S3	Case 3-Δt = 180 s	~2000	1210.8(28.6)	1020.6 (20.4)	1173.4 (151)	1320 (283.6)
S4	Case 3-Δt = 60s	~4000	3602.2(157)	3529.4 (86)	3885.6 (438)	4267.4 (817)

where the subscript denotes the location, b denotes the branch index, i denotes the cross-section index (see Fig. 1), e denotes the last cross-section of the branch, and α, β, ζ, ε, η, γ are the chasing coefficients. The details about the derivations of these coefficients can be found in Zhang and Shen (2007).

The next step is to reduce the number of unknowns by incorporating a boundary condition based on the mass conservation at each junction, as shown in Eq. (4). Akan and Yen (1981) showed that the energy equation could be approximated by the water stage equality when the flow at the junction is subcritical, as shown in Eq. (5). Hence, the water level at the junction node can be regarded to be the same as those at the nearest cross-sections of the branches linked to the junction. More complex conditions (Kesserwani et al., 2008b; Yuan et al., 2021; Yuan et al., 2022) are not considered in this paper.

$$\sum Q = \sum Q_{in} - \sum Q_{out} = 0 \tag{4}$$

$$Z_{in} = Z_{out} \tag{5}$$

where subscript *in* and *out* denotes inflow and outflow, respectively.

According to Eq. (5), the nodal water level Z_j (the subscript indicates the location of the node) can be used to represent the cross-sectional water levels that are directly related to the junction (for example, $Z_{1,6}$, $Z_{2,6}$ and $Z_{3,1}$). We can establish a linear relationship between the water level at a junction and those at its nearby junctions by substituting the relationship between the flow rate and the nodal water level, Eq. (3), into Eq. (4). The linear nodal water level equation is as follows:

$$u_j Z_j = \sum_{k=1}^{N_j} u_{jk} Z_{jk} + v_j \tag{6}$$

where u_j, u_{jk} and v_j are the linearized coefficients; u_j is a linear combination of the chasing coefficients β and γ; u_j is a linear combination of the chasing coefficients ζ and η; u_j is a linear combination of the chasing coefficients α and ε.

The above nodal water level equation, Eq. (6) can be established for each junction. Then, a system of global equations can be established, with the water levels at junction nodes as the basic unknowns:

$$[\mathbf{\Phi}] \times [\mathbf{Z}] = [\mathbf{S}] \tag{7}$$

where $\mathbf{\Phi}$ is the coefficient matrix; $\mathbf{S}$ is the right-hand vector;$\mathbf{Z} = [Z_1, Z_2, \cdots, Z_{NP}]^T$ is the vector containing the water level variables at all junctions, and *NP* is the total number of junction nodes.

The values of the junction water levels can be obtained by solving the above global equation system, i.e., Eq. (7). Once the end-node variables are found for a branch, they are substituted into the branch equations as boundary conditions to get the variables at interior nodes. In this study, the global equations are solved by the RWP method, which is a probabilistic approach. It is known that the probability of an event can be estimated by its frequency observed during a large number of experiments. The key to transforming the deterministic problem into a probabilistic problem is to establish a stochastic process whose statistical quantities are equivalent to the solution to the deterministic problem. These statistical quantities are calculated by implementing a statistical process. After taking enough samples, the approximate solution is obtained. In this study, the statistical quantities are obtained via Monte-Carlo simulation. A rigorous mathematical proof of the probabilistic representation is provided in the following subsection.

2.2. Theoretic basis of random walk path method

2.2.1. The link between transition probability formula and random walk path

Dividing both sides of Eq. (6) by u_j, Eq. (6) can be rewritten as Eq. (8), the transition probability formula between one junction and its adjacent junctions.

$$Z_j = \sum_{k=1}^{N_j} p_{jk} Z_{jk} + s_j \tag{8}$$

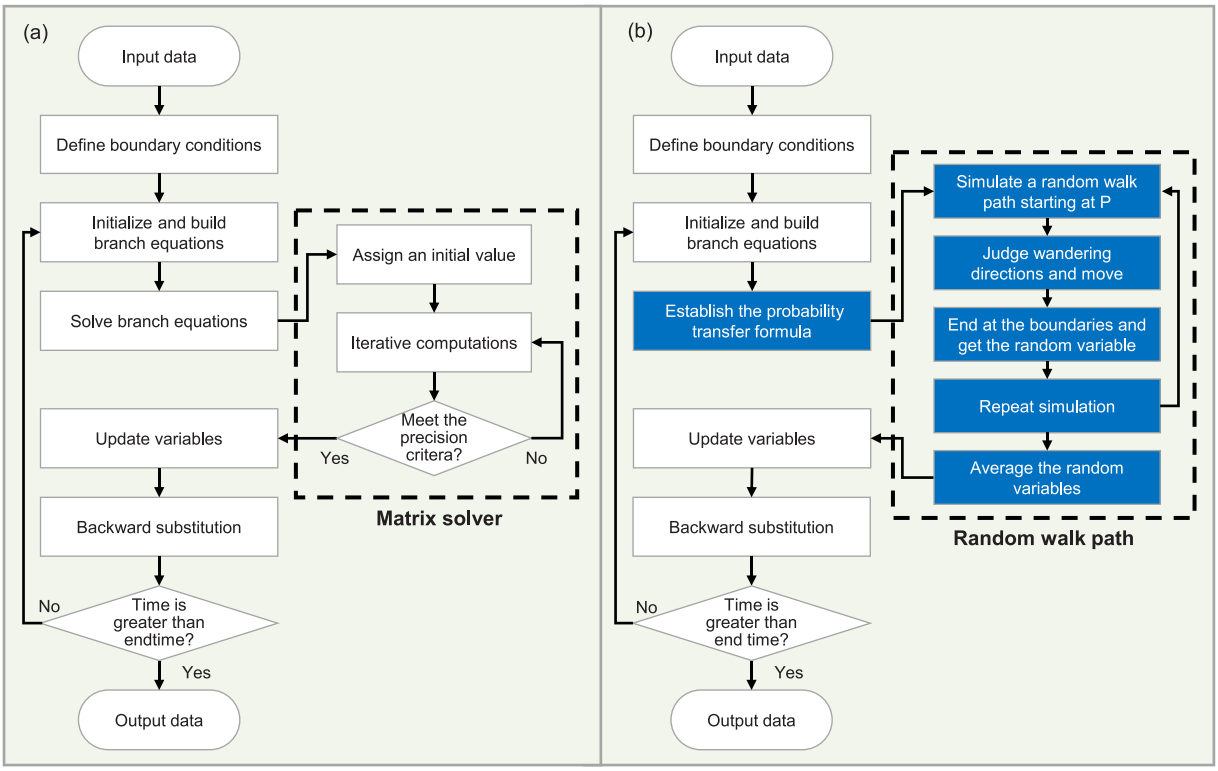

Fig. 3. (a) Flowchart of three-step algorithms with a traditional matrix solver; (b) Flowchart of RWP method. The main difference between the two flowcharts is marked in blue. (For interpretation of the references to color in this figure legend, the reader is referred to the web version of this article.)

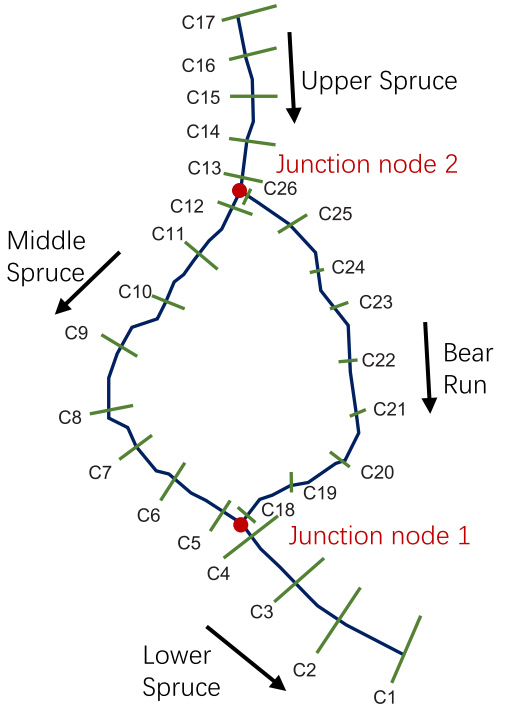

Fig. 4. Looped river system schematic, where C denotes the cross-section.

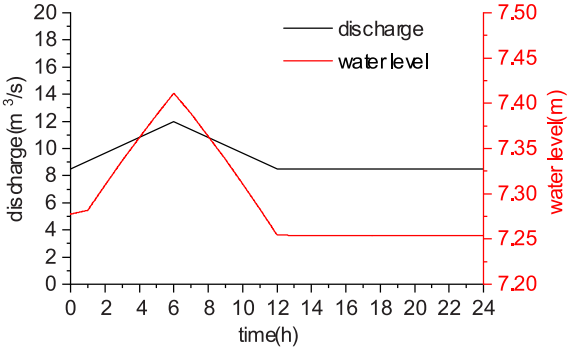

Fig. 5. Upstream boundary conditions for test 1 and test 2.

where $p_{jk} = u_{jk}/u_j$ denotes the transition probability; $s_j = v_j/u_j$is the source term. It is worth mentioning that two conditions of the transition probability formula are (1) $\sum_{k=1}^{N_j} p_{jk} = 1$, and (2) $0 \le p_{jk} \le 1$. The first condition can be met by normalization. While not all conditions satisfy the prerequisite of probability non-negativity, the requirements that the practical application should meet are detailed in Appendix B.

The transition probability between junction nodes is related to the strength of their correlation. When it is applied to a channel network, the transition probability can reveal the strength of the relationship between water levels at junctions. Such a strength might be related to the branch length, resistance, head difference and other factors between the adjacent junction nodes. If the transition probability approaches zero, the change of junction water level virtually does not affect the surrounding junctions. This can happen when the distance between the junction is long or the resistance is too large. The relevance of Eq. (8) can be understood from the perspective of the probabilistic process. Here, a simple example exhibits the relationship between the deterministic formula and the random walk path. Consider a simple river layout as seen in Fig. 2. It is assumed that the water levels at boundaries (Z_1, Z_2, Z_5, and Z_6) are already known, whereas the values at interior junction nodes (Z_3 and Z_4) are unknown. According to Eq. (8), the relationship between the water levels at junction nodes 3 and 4 can be written as

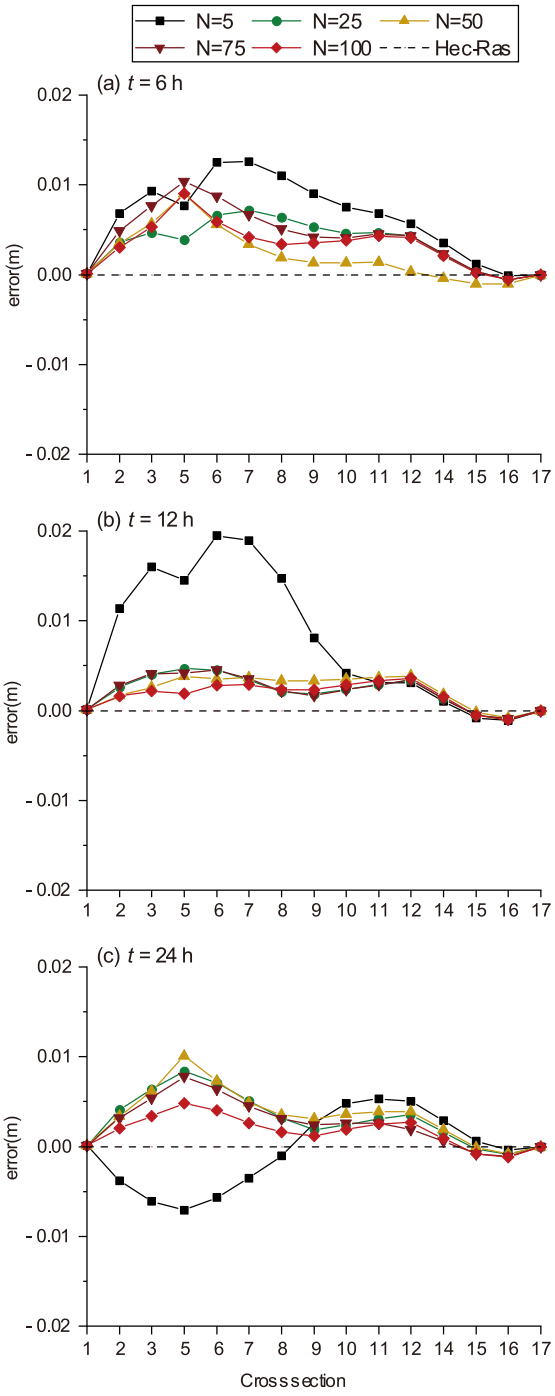

Fig. 6. Random walk solutions for water levels at $t = 6$ h, 12 h, 24 h with $N_{RS} = 5$, 25, 50, 75, 100: water-level-hydrograph boundary.

$$\begin{cases} Z_3 = p_{31}Z_1 + p_{32}Z_2 + p_{34}Z_4 + s_3 \\ Z_4 = p_{43}Z_3 + p_{45}Z_5 + p_{46}Z_6 + s_4 \end{cases} \tag{9}$$

From the perspective of a random process, p_{jk} can be deemed as the probability of a walker moving to junction node k corresponding to the subscript jk from junction node j. We can set a random walk scheme based on these probabilities. At node j, a walker can move to its adjacent junction nodes with probability p_{jk}; and the walker continues to move based on the transition probability until it arrives at the terminal, which may be node 1, 2, 5 or 6. Then, Z_3 can be expressed by the weighted average of the known boundary water levels. Assuming all the probabilities p_{jk} are 1/3, one can quickly solve Eq. (9) and then obtain Eq.

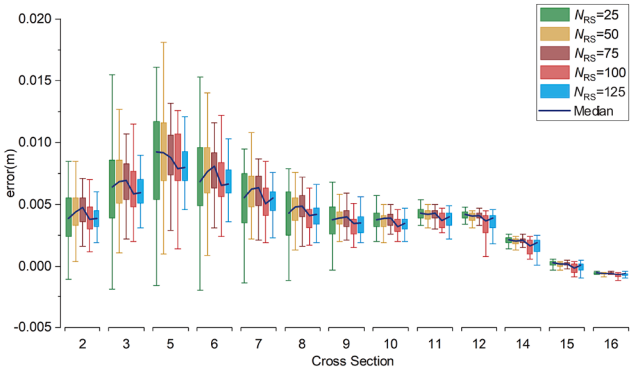

Fig. 7. Water level errors in random walk solutions at $t = 6$ h with $N_{RS} = 25$, 50, 75, 100, 150: water-level-hydrograph boundary condition.

(10). It is important to note that here the probability of 1/3 is assumed. In practice, the likelihood of the transfer varies from one direction to another. For this condition, the 3/8 and 1/8 are the likelihoods of walker starting from node 3 and ending at nodes 1 and 5, respectively. For node 4, the random variable at the junction can also be written in a similar form. In conclusion, the random variable Z_j at any junction node can be expressed as in Eq. (11).

$$\begin{cases} Z_3 = \frac{3}{8}Z_1 + \frac{3}{8}Z_2 + \frac{1}{8}Z_5 + \frac{1}{8}Z_6 + \frac{9s_3 + 3s_4}{8} \\ Z_4 = \frac{1}{8}Z_1 + \frac{1}{8}Z_2 + \frac{3}{8}Z_5 + \frac{3}{8}Z_6 + \frac{3s_3 + 9s_4}{8} \end{cases} \tag{10}$$

$$Z_j \approx \sum_{l=1}^{NT} p_l Z_l^{(\mathrm{T})} + \sum_{\{s_j\}} w_j s_j \tag{11}$$

where p_l denotes the existing probability; $Z_l^{(\mathrm{T})}$ is a known water level at a boundary (the subscript l indicates the position of the boundary, and the superscript T stands for "terminal"); NT is the number of boundary points; $\{S_j\}$ is the set of source items; $\sum_{\{s_j\}} w_j s_j$ is the cumulative impact of the source terms along the random walk path, w_j is the coefficient for the source term s_j.

Conventionally, the existing probabilities p_l and coefficients w_j are obtained through transformation equations such as Eq. (9). However, in a complex channel network, solving matrices directly is highly time-consuming. The Gaussian elimination procedure, the standard method for solving the linear equations, needs $O(n^3)$ arithmetic operations. For higher order matrix operations, stochastic algorithms such as the Monte-Carlo method can be used. Moreover, boundary effects can also be considered, which is demonstrated in Sec. 3.5.

2.2.2. A probabilistic representation of the solution of the global equations

To get the relationship between the random variable Z and the known water level values at boundaries, Monte-Carlo simulations are introduced in this study. For each simulation, a random walk path ν_p : $Path = P_1 \rightarrow P_2 \rightarrow \cdots \rightarrow P_{m-1} \rightarrow P_{\mathrm{T}}$, where the arrow $\rightarrow$ denotes the direction of movement, can be obtained, which starts from the point P_1, with an unknown water level, and terminates at an external boundary node P_{T}, with a known water level. The stochastic representation of the solution implies a Brownian path until the walker arrives at the boundary. Note that the subscript here indicates an arbitrary intermediate location of the walker rather than a precise location. One can obtain many random walk paths by multiple simulations, and these paths vary with simulations.

Define a random variable ξ corresponding to a random route as

$$\xi = g(\nu_P) = s(P_1) + s(P_2) + \cdots + s(P_m) + f(P_{\mathrm{T}}) \tag{12}$$

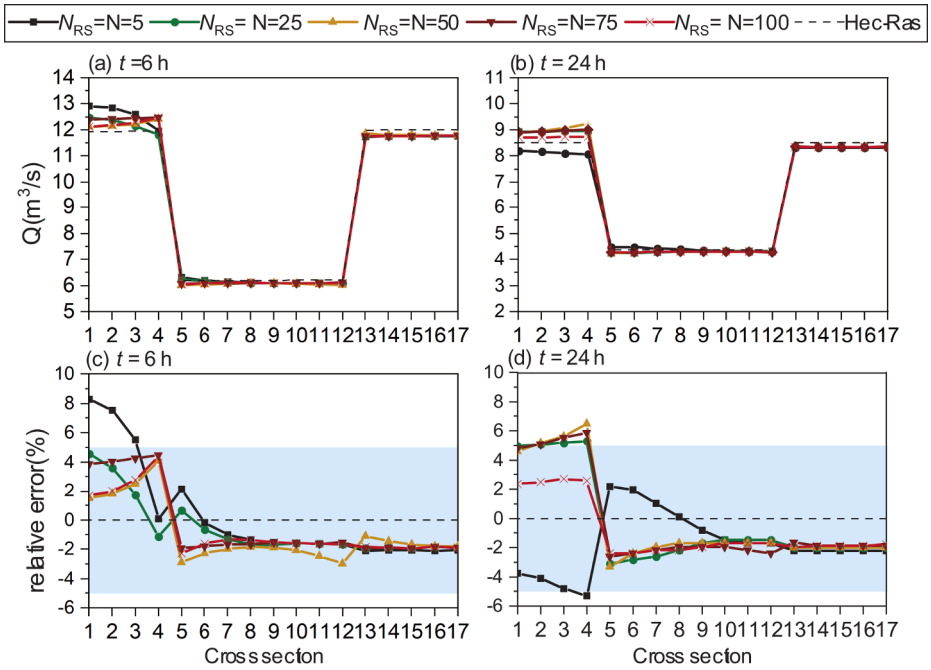

Fig. 8. (a) (b) RWP simulated discharge at $t = 6$ h, 24 h and (c) (d) the relative error at $t = 6$ h, 24 h with $N_{RS} = 5$, 25, 50, 75, 100: water-level-hydrograph boundary.

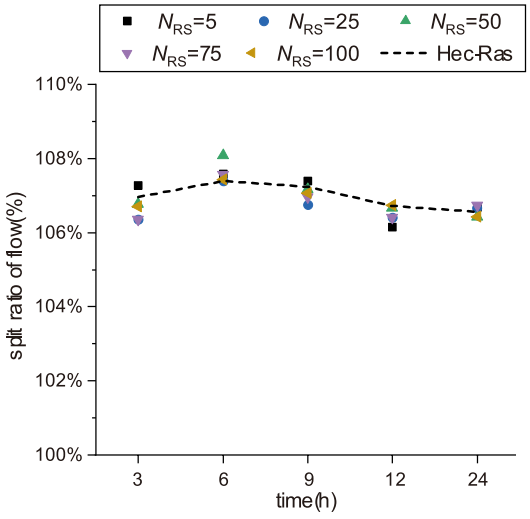

Fig. 9. Split ratio of flow (Middle Spruce to Bear Run) at junction node 1 of the looped river network.

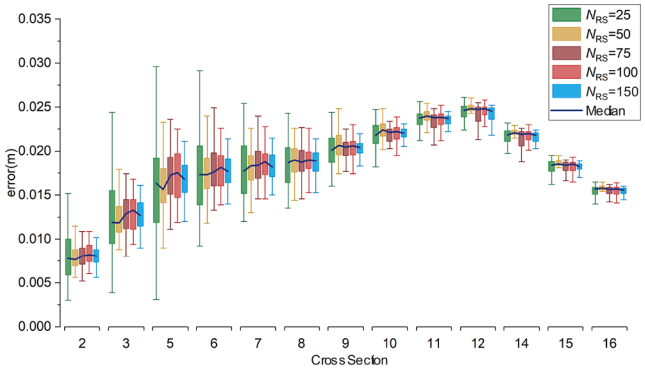

Fig. 10. Water level errors in random walk solutions at $t = 6$ h with $N_{RS} = 25$, 50, 75, 100, 150: discharge hydrograph boundary.

where $g(\cdot)$ and $f(\cdot)$ are functions of the random route and boundary points, respectively; $s(P_m)$ is equal to the source term for the m-th node along the random path passes.

Through multiple trials, we can get a set of random variables $\Xi = \{\xi_1, \cdots, \xi_n, \cdots, \xi_{N_{RS}}\}$ corresponding to different random routes. The probabilistic representation of the solution at junction node P_1 is

$$Z(P_1) = E(\Xi) \tag{13}$$

In other words, the defined random variable $\Xi = \{\xi_1, \cdots, \xi_n, \cdots, \xi_{N_{RS}}\}$ has a mathematical expectation equal to the water level at the junction node. If Eq. (13) holds, then a statistical test can be performed to estimate the value of this variable $Z(P_1)$. One random variable's value can be obtained from one random walk, and N_{RS} random walks simulations yield N_{RS} random variable values, with the average value serving as an approximation of $Z(P_1)$.

The following is a formal proof that the mathematical expectation of random variables is indeed the same as the problem's solution. Depending on the location of the starting point, it can be divided into two cases:

Case 1: If the starting point of a walker is a boundary node P_T, then it stays at point P_T. So, the value of the defined variables ξ can be formulated as:

$$\xi = g(\nu_{P_T}) = f(P_T) \tag{14}$$

Case 2: If the walker does not start from a boundary node P_T, then we only need to prove Eq. (15) to justify Eq. (13).

$$E(g(\nu_{P_T})) = \sum_{k=1}^{N_j} p_{jk} Z(P_{jk}) + s(P_1) \tag{15}$$

The random process ν_p can be thought of as consisting of two routes, namely $P_1 \rightarrow P_{1k}$ and $\nu_{p_{1k}} : P_2 \rightarrow P_3 \rightarrow \cdots \rightarrow P_{m-1} \rightarrow P_T$. For the second route $\nu_{p_{1k}}$, the random variable ξ should have the value

$$\xi = g(\nu_{p_{1k}}) = s(P_2) + \cdots + s(P_m) + f(P_T) \tag{16}$$

From the above Eq. (12) and Eq. (16), it is clear that:

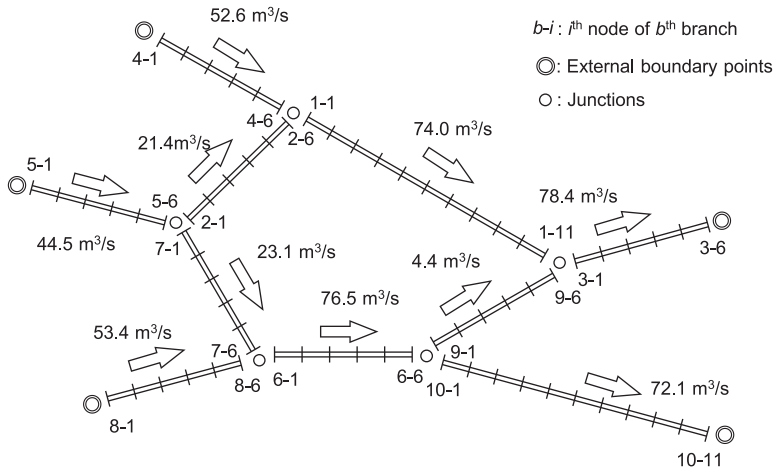

Fig. 11. Channel network of test case 2.

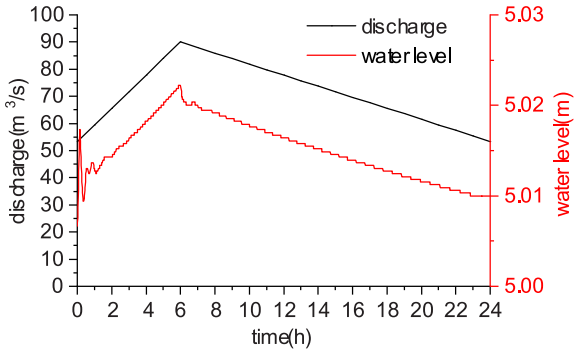

Fig. 12. Upstream boundary condition at node 8–1 for channel network.

$$g(\nu_p) = g(\nu_{p_{1k}}) + s(P_1) \tag{17}$$

According to the mathematical properties of the expectation of the discrete random variables, the right side of the Eq. (12) can be expressed as:

$$\begin{aligned} E(g(\nu_p)) &= \sum_{\{\nu_p\}} g(\nu_p)\cdot Pr(\nu_p) \\ &= \sum_{k}^{N_j} \sum_{\{\nu_{p_{1k}}\}} \left[g(\nu_{p_{1k}}) + s(P_1)\right]\cdot Pr(P_1 \to P_{1k})\cdot Pr(\nu_{p_{1k}}) \\ &= \sum_{k}^{N_j} p_{1k} \sum_{\{\nu_{p_{1k}}\}} \left[g(\nu_{p_{1j}}) + s(P_1)\right]\cdot Pr(\nu_{p_{1k}}) \\ &= \sum_{k}^{N_j} p_{1k} \sum_{\{\nu_{p_{1k}}\}} g(\nu_{p_{1k}})\cdot Pr(\nu_{p_{1k}}) + \sum_{k}^{N_j} p_{1k} s(P_1) \sum_{\{\nu_{p_{1k}}\}} Pr(\nu_{p_{1k}}) \end{aligned} \tag{18}$$

In the above proof, $Pr(\nu_p)$ is the probability that the walker moves along the route ν_p, $Pr(P_1 \to P_{1k})$ is the probability with which the walkers moves from point P_1 to point P_{1k}, which is equal to p_{1k}. Since $s(P_1)$ has nothing to do with k, Eq. (18) can be rewritten as:

$$\begin{aligned} E(g(\nu_p)) &= \sum_{k}^{N_j} p_{1k} \sum_{\{\nu_{p_{1k}}\}} g(\nu_{p_{1k}})\cdot Pr(\nu_{p_{1k}}) + \sum_{k}^{N_j} p_{1k} s(P_1) \\ &= \sum_{k}^{N_j} p_{1k} u(P_{1k}) + s(P_1) \end{aligned} \tag{19}$$

Thus, Eq. (15) is proved, which means that Eq. (13) holds good.

2.3. Numerical evaluation of water level functions via RWP

Theoretically, the function $f(P_T)$ in Eq. (12) can be arbitrary, and here it is taken as the known water level $Z_l^{(T)}$ at the boundary. The

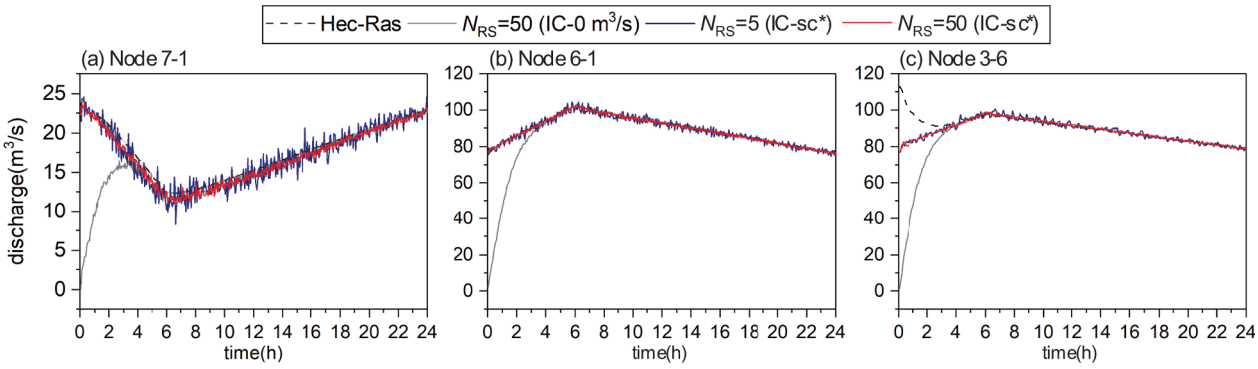

Fig. 13. Discharges at node (a) 7–1, (b) 6–1, and (c) 3–6 with $N_{RS} = 5$, 50 with different initial conditions, as compared with the Hec-Ras simulations with steady flow as the initial condition sc*.

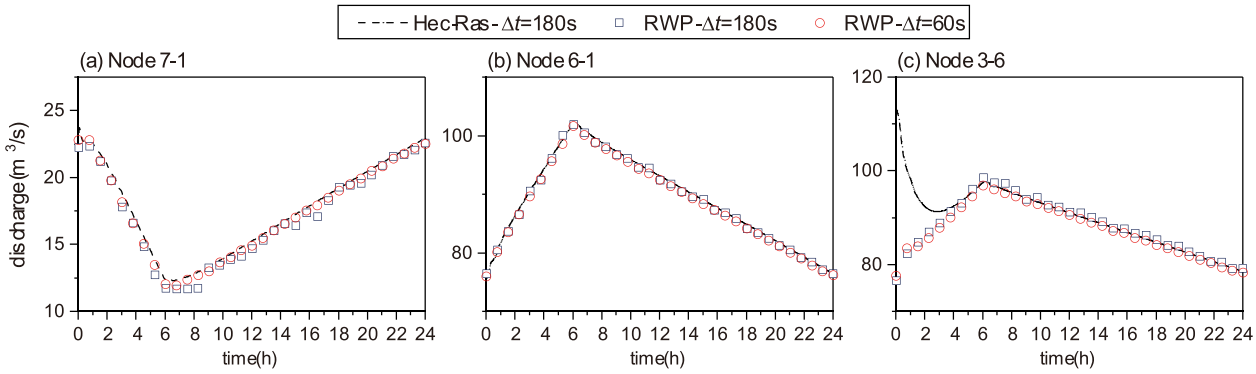

Fig. 14. Discharge at node (a) 7–1, (b) 6–1, (c) 3–6 with N_{RS} = 50 with Δt = 180 s and 60 s compared to simulated values by Hec-Ras with water-level-hydrograph boundary.

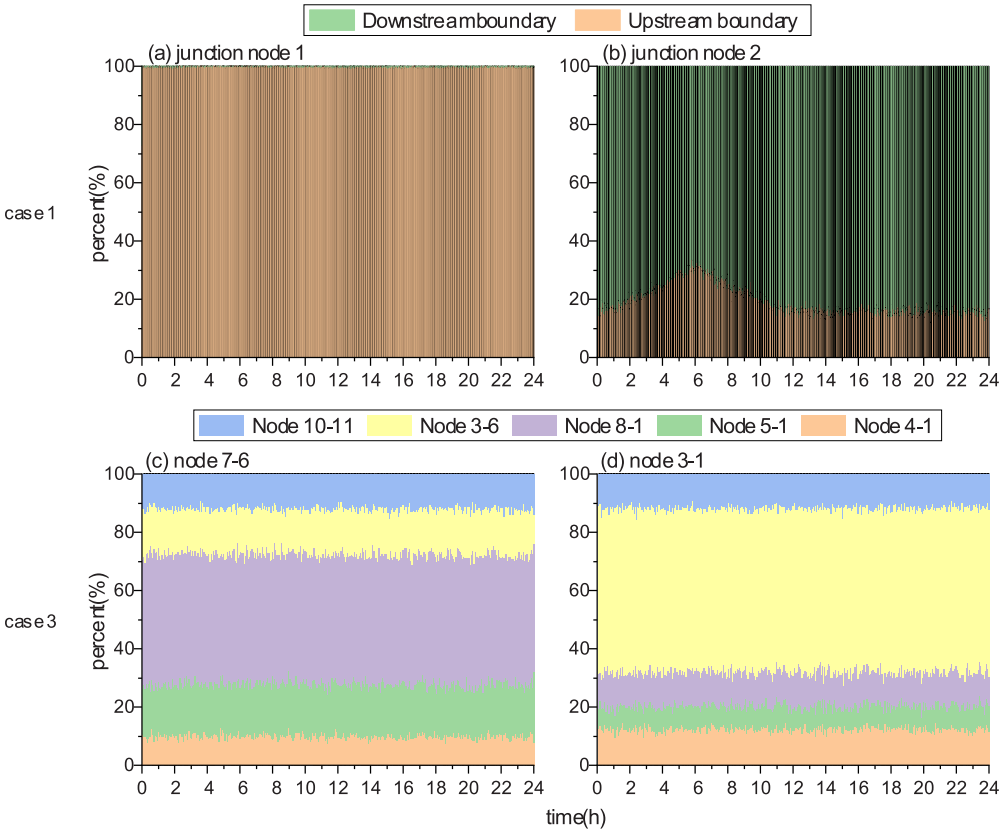

Fig. 15. Boundary influence capacities, i.e., the impacts of the different boundary conditions on the water levels at junction nodes, in (a) (b) case 1 and (c) (d) case 3.

average value of all the random variables (ξ_1, …,ξ_n, …,$\xi_{N_{RS}}$) can be deemed equal to the mathematical expectation if the number of RWP simulations (N_{RS}) is large enough, according to the large number theorem. After conducting a large number of Monte Carlo simulations one can get

$$Z_j \approx \frac{1}{N_{RS}}\sum_{n=1}^{N_{RS}}\xi_n = \frac{1}{N_{RS}}\sum_{l=1}^{NT} d_l Z_l^{(T)} + \frac{1}{N_{RS}}\sum_{\{s_j\}} h_j s_j \tag{20}$$

where T denotes the terminal value; d_l and $Z_l^{(T)}$ is the number of walkers ending up at the external boundaries and the corresponding terminal water level, respectively; $\sum_{\{s_j\}} h_j s_j$ is the source accumulations in all realizations, and h_j is the number of occurrences of walkers at the corresponding source item point. The values of d_l and h_j are obtained statistically.

In summary, realization of a RWP simulation can be conducted according to the following workflow:

(1) Define the basic global equation and get the transition formulation.

(2) Define the random wandering function Eq. (12).

(3) Conduct Monte-Carlo numerical tests:

a. Place a walker at the point P and begin to simulate a random walk path starting from point P.

b. Generate a random number with a value in the interval (0,1), and judge wandering directions by comparing it to the intervals of transfer probabilities (1, p_{j1}), …, ($\sum_{k=1}^{k=n_k-1} p_{jk}$, $\sum_{k=1}^{k=n_k} p_{jk}$), …, ($\sum_{k=1}^{k=N_j-1} p_{jk}$,1), where n_k is the index of junction node connected to junction node j. The walker is then displaced to a neighboring junction node based on the wandering direction.

c. The walker is then continuously displaced until it reaches an external boundary. Once one random walk path simulation is accomplished, we can retrieve one simulated value ξ_n.

d. Repeat the preceding steps to simulate a large number (i.e., N_{RS}) of random walkers and obtain N_{RS} simulated random values.

e. Average the random variables to estimate the expected water level.

(4) Update the variables and proceed with backward substitution of the branch equations to calculate the remaining unknown variables at the interior cross-sectional nodes.

The flowcharts of the traditional three-step method and RWP method are illustrated in Fig. 3. For comparison, the main differences between the two methods are marked in blue color.

2.4. Boundary condition

The water-level-hydrograph function at the boundary can be directly given as the value of the water level itself. However, a special technique is required to treat the discharge-hydrograph boundary. Taking the channel network in Fig. 2 as an example, suppose that the boundary type at point 1 changes from the water-level-hydrograph to a discharge-hydrograph. According to Eq. (3), the flow rate at the boundary can be linearly expressed in terms of the water levels as $Q_1 = \alpha_1 + \beta_1 Z_1 + \zeta_1 Z_3$. By rewriting Eq. (3), a relationship between the water levels at the boundary and its adjacent internal junction nodes, i.e., point 1 and point 3, can be obtained:

$$Z_1 = p_r Z_3 + p_a \frac{Q_1 - \alpha_1}{\beta_1 + \zeta_1} \tag{21}$$

where $p_r = -\zeta_1/\beta_1 < 1$ and $p_a = 1 - p_r$. The subscript r and a denotes reflection and absorption, respectively; α_1, β_1, and ζ_1 are the chasing coefficients associated with the branch 1.

According to the theory proposed by Maire and Nguyen (2016), $(Q_1 - \alpha_1)/(\beta_1 + \zeta_1)$ can be added to the water level at point 1, which converts the discharge at the boundary into a virtual water level $Z_1^{'} = (Q_1 - \alpha_1)/(\beta_1 + \zeta_1)$. From the probabilistic point of view, there is a likelihood that the water levels at point 1 and point 3 are identical. In such a circumstance, the walkers that advance to point 1 are all returned to point 3. In addition, there is a chance that the water level at point 1 is equal to the virtual water level $Z_1^{'}$, in which case the walkers stop moving when they hit boundaries, because the water levels are already known there. We define the aforementioned processes as reflection and absorption. We can then specify how the walkers should react when they hit different types of boundaries in Monte-Carlo simulations.

In the case of the water level boundary, the walker gets simply absorbed while meeting the boundary/terminal points P_T. Meanwhile, the function of the boundary $f(P_T)$ is equal to the water level at point P_T, i.e., $f(P_T) = Z_{P_T}$.

In the case of the discharge-hydrograph boundary, the walker will get reflected to an adjacent junction node with the probability p_r,or be absorbed with the probability p_a when it meets the boundary. When the walker is absorbed, the calculation flowchart is the same as above. The function of the discharge-hydrograph boundary is determined by the virtual water level at the boundary point, i.e., $f(P_T) = Z_{P_T}^{'}$. When $\zeta = 0$, the discharge-hydrograph boundary is equivalent to the water-level-hydrograph boundary and all walkers are absorbed by the boundary. To summarize, the difference between the discharge boundary and the water level boundary lies in the probability of reflection.

After computing the water levels at internal junctions, the real water levels at the boundary can be obtained by substituting those at adjacent junction nodes through Eq. (21). The rating curve boundary condition too can be linearized and treated in a similar way. By specifying the initial water level and initial flow rate in the channel system, the initial condition is provided (Li et al., 2020; Pu et al., 2012).

3. Numerical results and discussion

To assess the performance of the RWP method, three numerical tests are presented in this section. Hec-Ras (Hydrologic Engineering Center River Analysis System) is an engineering model for the solution of the Saint-Venant equations, which was developed by the U.S. Army Corps of Engineers. Hec-Ras has been verified in numerous applications (Liu and Hodges, 2014) and is used to generate benchmark solutions in this article to evaluate the efficacy of RWP method. The first two benchmark tests are used to test the performance of the RWP method for the looped channel system under different boundary conditions. The third one is to test the performance for the dendritic and divergent channel system and to show the advantages of terminal weights in quantitatively evaluating the influence of the conditions at various boundaries on the channel's interior flows.

3.1. Test Case 1

The applicability of the RWP method is first checked in the context of a looped channel network, as seen in Fig. 4 (Brunner, 2018). The split in the main channel (Spruce Creek) forms two streams (Bear Run and Middle Spruce Creek) which later join together. Spruce Creek is approximately 610 m long, and Bear Run is approximately 450 m long. The Manning's roughness coefficient for the main channel and flood plain are 0.04 s $m^{-1/3}$ and 0.08 s $m^{-1/3}$, respectively. The reader may refer to the Hec-Ras application guide for more detailed geometric data.

The looped network example in the Hec-Ras application manual considers a steady-state setup . To study the characteristics of the RWP model under unsteady conditions, with the pure water-level-hydrograph boundaries, the steady discharge of 8.459 m^3/s at the upstream boundary was changed to be time-variant in Hec-Ras. The final upstream boundary condition used was the water-level-hydrograph calculated by Hec-Ras, as shown in Fig. 5. The downstream condition remains the same with a constant water level of 6.66 m. The initial condition of water level is 6.66 m throughout the whole river system. The calculation duration is 24 h and Δt is 60 s. The results are compared with those from Hec-Ras. For the reader's convenience, the boundary cross-sections and types of boundary conditions involved in this study are listed in Table 1.

3.1.1. Errors of the RWP method

The errors were found to generally fall as the number of random experiments increases. The results of RWP computations are compared with the Hec-Ras solutions at time $t = 6$ h, $t = 12$ h, and $t = 24$ h in Fig. 6. The RMSE (root mean square error) and MAPE (mean absolute percentage error) are adopted to quantify the deviation of the RWP solutions from the Hec-Ras solutions. The RMSE is defined as $\mathrm{RMSE} = \sqrt{\sum_{j=1}^{NP}\left(Z_j^{(rwp)} - Z_j\right)^2 / NP}$ where $Z_j^{(rwp)}$ is the water level at the j-th junction node and Z_j is the "true" value calculated by Hec-Ras. The MAPE is defined as $\mathrm{MAPE} = \sum_{j=1}^{NP}\left|\left(Z_j^{(rwp)} - Z_j\right)/Z_j\right| / NP$, where NP is the total number of junction nodes. The corresponding RMSE and MAPE are listed in Table 2. If the number of random experiments is 5, the errors are relatively large. The errors decrease as the number of random experiments increases. If N_{RS} is increased to 100, the RMSE and the MAPE at $t = 12$ h decrease from 0.0105 m to 0.0029 m and from 0.13% to 0.04%, respectively (see Table 2). The error distribution along the channel at fixed times ($t = 6$ h, for example, Fig. 6(a) below) suggests that $N_{RS} = 100$ results in larger errors compared to $N_{RS} = 50$ (RMSE increases from 0.0068 m to 0.007 m). This may be due to the random errors of the stochastic model itself. If N_{RS} increases to a certain threshold value, the calculated results gradually converge, and the computational errors stabilize within a narrow range. The stabilized computational error is comparable to the magnitude (10^{-3}) of the random error.

To study the error of the stochastic process itself, 50 calculations

were repeated with the same number of random simulations. The results are presented in Fig. 7, using Hec-Ras results as reference values. The median was chosen because it can better describe the central tendency of the errors to avoid the influence of extreme values. If the number of random simulations is small, there exists considerable instability in the results. For example, the fluctuations of flow errors at cross-section C5 are approximately 0.03 m for $N_{RS} = 25$ and fall to 9×10^{-3} m when $N_{RS} = 150$. It can be concluded that when the number of random simulations is larger, the range of fluctuations formed by the random process gets smaller. However, if the number of random simulations increases, the convergence error stabilizes. This is expected because more simulations eliminate the influence of random errors according to the Law of Large Numbers. However, increase in the number of walks beyond a certain level does little to improve the accuracy. Too little simulation leads to large random errors, and too many simulations take too much of time. We should, therefore, choose a moderate simulation number N_{RS} depending upon the accuracy needed.

3.1.2. Discharge and flow partition

The RWP predicted discharges are compared with the Hec-Ras solutions at $t = 6$ h and $t = 24$ h in Fig. 8. Unsurprisingly, an increase in the simulation number reduces the errors of the solution. When $N_{RS} = 100$, the relative flow error is in the range of ±5% (see Fig. 8). Channel bifurcations cause discharge apportioning, and the prediction of flow partitioning at channel networks is important (Dong et al., 2020). Therefore, the split ratio of flow which shows the percentage of discharge in Middle Spruce to that in Bear Run is also computed. Fig. 9 shows the variation in the split ratio of flow over time for different numbers of random simulations. Even when $N_{RS} = 5$, the split ratio is close to the simulated values by Hec-Ras. This suggests that if we want to know quickly the partitioning of flow, it would suffice to choose a smaller number of simulations.

3.2. Test Case 2

Here, all settings are the same as in Case 1 except that we change the upstream boundary conditions to a discharge-hydrograph. The upstream discharge-hydrograph is the same as that in Section 3.1 (see Fig. 5). Following the above analysis, the solutions still did have random errors (see Fig. 10).

Not surprisingly, the random error fades away as N_{RS} grows. Hence, it is important to choose number of random simulations suitably under the prevailing boundary conditions. The error distribution in random walk solutions seems to be different and shows an opposite trend in Case 2 compared with Case 1. In Case 2, the error at the cross-section near the upstream boundary is larger, which may have resulted as the virtual water level was derived from discharge, referred to in Subsection 2.4.

3.3. Test case 3

A hypothetical network consisting of the dendritic and divergent channel system is shown in Fig. 11. Fig. 11 shows a discharge with a constant condition that has been pre-calculated by Hec-Ras as an initial discharge condition. Relevant features of the channels are given in Table 3. The upstream (node 4–1 and node 5–1) and downstream (node 3–6 and node 10–11) water level boundary conditions are held constant at 5.01 m and 5 m, respectively. The boundary condition at node 8–1 is firstly specified with a non-constant discharge process in Hec-Ras, as illustrated in Fig. 12. Same as in test Case 1, Case 3 uses the water-level-hydrograph (see Fig. 12), calculated by Hec-Ras, as all other boundary conditions.

The water level errors can be ignored in this test case because the magnitude of the change in water level is minimal. For simplicity, we only demonstrate the results of the discharge calculation here. The discharges at node 7–1, node 6–1 and node 3–6 are compared to the simulated values of Hec-Ras as illustrated in Fig. 13 and Fig. 14 . They show the effects of different parameters.

Fig. 13 presents the effect of the number of simulations and initial conditions on the calculation results. The initial condition of water level is 5 m throughout the whole channel system. Two initial conditions of discharge in the channel network are tested here: (1) steady condition (shown in Fig. 11), calculated by Hec-Ras with constant water levels of 5.01 m and 5 m at the upstream and downstream boundaries, respectively; (2) $Q = 0$ m^3/s along all the branches. In the case of initial condition (1), when $N_{RS} = 5$ and 50, the discharge values calculated by RWP match well with those calculated by Hec-Ras. Although there are apparent fluctuations when $N_{RS} = 5$, the calculated discharge tended to be, to a certain extent consistent with the solution given by Hec-Ras. The stochastic error can be eliminated or decreased by smoothing techniques. In the case of initial condition (2), the fairly large error at the beginning is due to the inaccurate initial conditions. Studies have pointed out that the three-step algorithms could be unstable when the initial conditions are inaccurate or the time step is not carefully chosen (Zhu et al., 2011 and references therein). However, if we are more concerned with the constant flow state of the channel network under hydraulic control operation, this is not a major issue. The inadequate initial conditions could be trivial and the solution is affected only by the imposed boundary conditions after the spin-up time. The effect of the time step is illustrated in Fig. 14. According to Fig. 14, the time step barely affects the accuracy and convergence.

3.4. Boundary effects

In Subsection 2.2, it was mentioned that the internal nodal water level can be expressed by linear combinations of water levels at known boundaries. The terminal weight d_k/N_{RS} describes the possibility of walkers, starting from the calculated point, to end at a certain boundary. This random walk process is a Markov chain and is reversible. As a result, the path starting from an internal node that ends at a boundary is equivalent to that starting from the boundary and ending at the interior node. In numerous experiments, the frequency of paths from a boundary that arrive at internal nodes reveals the extent of the boundary's influence on the water level at those nodes. Then, the boundary effect, which specifies the contribution of the boundary condition to the water level at a junction node, can be reflected by the terminal weights. The boundary effect found in Case 1 and Case 3 are illustrated in Fig. 15. Case 1 and Case 2 have very similar results about the boundary effect, so Case 2 is not discussed here.

There are only two boundaries in Case 1. Upstream condition plays a leading role in influencing the water level in node 1. In other words, this point is hardly influenced by the downstream backwater effect. In contrast, junction node 2 is affected by the combination of upstream and downstream conditions. The upstream effect first increases and then decreases consistently in accordance with the upstream flow rate trend. In Case 3, the boundary effects compete with each other. This phenomenon may arise from the backwater effects, especially in the plain river network area. Case 3 also shows that the boundary effects barely vary, although the boundary condition at node 8–1 is time-variant. This near constant influence may result as the water level fluctuations are small for low discharge conditions in the plain river network area. The terminal weights can act as a simple and effective tool in the sensitivity analysis of flooding problems (Mazzoleni et al., 2018; Pappenberger et al., 2006; Tang et al., 2020).

3.5. Computational time and efficiency

Computational efficiency is one of the most critical aspects of an algorithm. Table 4 lists the computational times of the RWP method, Hec-Ras and the traditional three-step method. Owing to the randomness, the repetition calculation time of the RWP method is not always the same. The values of the RWP method listed in Table 4 are the averages of 50 runs. The numbers in brackets indicate the times for solving the

equations, excluding the computational costs for equation initialization and problem setup. As mentioned above, the main difference between the RWP method and the conventional three-step method is matrix solving (Fig. 3). Hec-Ras uses a sparse matrix solution technique to solve the equations directly rather than reduce the order of the matrix (Brunner, 2016). To better study the efficiency of RWP, the traditional three-step method with the Gaussian elimination algorithm as a global matrix solver (Sen and Garg, 2002) is also used here for the comparison. All the numbers listed here exclude the time of post-processing.

Table 4 shows that the computational cost increases as N_{RS} increases. In both cases, the computational efficiency of the traditional three-step and RWP methods seems larger than that of Hec-Ras. As the code is not open-source, we can only presume that Hec-Ras adopts the approach of solving the system of equations directly. If $N_{RS} = 5$, the computational cost of the RWP method is the lowest. For $N_{RS} = 50$ and $N_{RS} = 100$, RWP is less efficient than the traditional three-step method, which is based on the linear matrix solver. Owing to the reflectivity of the flow boundary, walkers may be reflected at the boundary, thereby increasing the wandering time. Therefore, the computational times of the test cases with discharge-hydrograph boundary conditions were generally longer than those with water-level-hydrograph boundary conditions. However, the marginally higher cost of the RWP method in Table 4 does not give the full story of the RWP method in comparison with the traditional method. Due to the inherent properties of the Monte-Carlo simulation, the RWP method is more robust and suitable for parallel computation. A recent study demonstrated that the time cost can be significantly reduced by up to 92.6% by applying the RWP method to transient groundwater flow problems (Nan et al., 2020). Therefore, the RWP computation has a great potential for speedup. One can choose the number of random simulations depending on the required precision. In some specific cases, it is essential to know quickly the split ratio of flow and the general trend of changes in the flow. In that case, a small N_{RS} will be appropriate because it requires a short computational time.

The high computational efficiency is required for repeated simulations during the process of optimization in water resources management (Tian et al., 2019; Xu et al., 2011). Although the RWP method has no obvious advantages in a single simulation, the total computational costs in case of repeated simulations are expected to be greatly reduced thanks to the physical meaning of the terminal weights mentioned in Sec. 3.4. They can be used in advance to reduce the computational burden by imposing constraints to the ranges of parameters, which can instantly disregard pumps that have little effects on the internal water levels. They can also be used to rank the pumping effectiveness.

4. Conclusions

In this study, a random walk path method was developed for unsteady flows in open channel networks considering different boundary conditions. It can provide reliable results for flows in both looped and dendritic channel networks. This method skips the global matrix solution and quickly yields the junction water levels by adopting Monte-Carlo simulations. Hence, this method requires smaller computer storage than the traditional three-step method.

This method's computational efficiency depends upon the number of simulations and the length of the walk. The reflectivity of the discharge boundary leads to an increase in the walking length, thereby increasing the computation time as compared with the pure water-level-hydrograph boundary. Although larger number of random simulations improves the precision, doing this increases the computational time. It is necessary to choose this parameter N_{RS} aptly by considering the trade-off between precision and computational efficiency. A small number of random simulations such as $N_{RS} = 5$ seems to be a good choice when a quick rough estimate of the flow is needed. In the future, parallel algorithms can be implemented to improve the speed of computation.

Furthermore, the RWP is able to quantify the water level dependence among junctions. The by-product of the RWP method is the terminal weights which can be used to quantitatively evaluate the influence of the conditions at various boundaries on the channel's interior flows. Hence, one can estimate the area flooded due to the backwater effects. Furthermore, these quantitative assessments can be useful to optimize the operations of hydraulic structures to reduce flood hazards. For river networks controlled by numerous sluice gates and pumps, the location of such engineering devices which play key roles can then be easily identified. Therefore, this method is able to improve the computational efficiency in the optimization phase.

Additional studies will be carried out in future to better understand the properties of the terminal weights. For time-invariant weights, the linearized water level relationships can be pre-calculated in engineering applications. It will then be possible to develop a RWP framework that undertakes efficient recalculations of the flows subjected to different combinations of the boundary conditions.

Declaration of Competing Interest

The authors declare that they have no known competing financial interests or personal relationships that could have appeared to influence the work reported in this paper.

Data availability

Data will be made available on request.

Acknowledgements

This research was funded by National Key R&D Program of China (Grant No. 2022YFC3200032), the National Natural Science Foundation of China (Grant Nos. U2040205, U2240209, and 52079044), the 111 Project (Grant No. B17015), and the Fok Ying Tung Education Foundation (Grant No. 520013312). The authors would like to thank Professor Bidya Sagar Pani of the Indian Institute of Technology-Bombay for his help in revising this work and thank Dr. Haitong Zhang for his help in computer programming. Thanks are also extended to Dr. Hao Cao of Hohai University and Professor Jiabiao Wang of Sun Yat-Sen University for their valuable advice.

Appendix A. Coefficients in the discretized Saint-Venant equations

$$as_1 = cs_1 = \theta \tag{A1}$$

$$bs_1 = -ds_1 = \frac{\Delta x}{4\Delta t}(L_{t_i} + L_{t_{i+1}}) \tag{A2}$$

$$es_1 = Q_{i+1} - Q_i + as_1 Q_i + bs_1 Z_i - cs_1 Q_{i+1} - ds_1 Z_{i+1} \tag{A3}$$

$$as_2 = \theta|Q_i| + \frac{1}{4g}(D_i^2 + D_{i+1}^2)\left(\frac{1}{A_i} + \frac{1}{A_{i+1}}\right)\left(\frac{1}{2\Delta t} + \frac{2\theta}{\Delta x}V_i\right) \tag{A4}$$

$$bs_2 = \frac{1}{2}\left(D_i^2 + D_{i+1}^2\right)\left\{\frac{\theta}{\Delta x} + \frac{1}{2g}\left(\frac{1}{A_i} + \frac{1}{A_{i+1}}\right)\left(-\frac{\theta}{\Delta x}V_i^2 L_{t_i}\right) + \left(-\frac{\theta}{2g}\frac{L_{t_i}}{A_i^2}\right)\left[\frac{1}{\Delta x}\left(V_i Q_i - V_{i+1}Q_{i+1}\right)\right]\right\} + \theta D_i \frac{KR^{2/3}}{3}\left(5L_t - 2R\frac{\partial P}{\partial z}\right)_i \left\{\frac{Z_i - Z_{i+1}}{\Delta x} + \frac{1}{2g}\left(\frac{1}{A_i} + \frac{1}{A_{i+1}}\right)\left[\frac{1}{\Delta x}\left(V_i Q_i - V_{i+1}Q_{i+1}\right)\right]\right\} \tag{A5}$$

$$cs_2 = -\theta|Q_{i+1}| - \frac{1}{4g}\left(D_i^2 + D_{i+1}^2\right)\left(\frac{1}{S_i} + \frac{1}{S_{i+1}}\right)\left(\frac{1}{2\Delta t} - \frac{2\theta}{\Delta x}V_{i+1}\right) \tag{A6}$$

$$ds_2 = -\frac{1}{2}\left(D_i^2 + D_{i+1}^2\right)\left\{-\frac{\theta}{\Delta x} + \frac{1}{2g}\left(\frac{1}{A_i} + \frac{1}{A_{i+1}}\right)\left(\frac{\theta}{\Delta x}V_{i+1}^2 L_{t_{i+1}}\right) + \left(-\frac{\theta}{2g}\frac{L_{t_{i+1}}}{A_{i+1}^2}\right)\left[\frac{1}{\Delta x}\left(V_i Q_i - V_{i+1}Q_{i+1}\right)\right]\right\} - \theta D_{i+1}\frac{KR^{2/3}}{3}\left(5L_t - 2R\frac{\partial P}{\partial z}\right)_{i+1}\left\{\frac{Z_i - Z_{i+1}}{\Delta x} + \frac{1}{2g}\left(\frac{1}{A_i} + \frac{1}{A_{i+1}}\right)\left[\frac{1}{\Delta x}\left(V_i Q_i - V_{i+1}Q_{i+1}\right)\right]\right\} \tag{A7}$$

$$es_2 = -\frac{1}{2}\left(Q_i|Q_i| + Q_{i+1}|Q_{i+1}|\right) - \frac{1}{2}\left(D_i^2 + D_{i+1}^2\right)\left\{\frac{Z_i - Z_{i+1}}{\Delta x} + \frac{1}{2g}\left(\frac{1}{A_i} + \frac{1}{A_{i+1}}\right)\left[\frac{1}{\Delta x}\left(V_i Q_i - V_{i+1}Q_{i+1}\right)\right]\right\} + as_2 Q_i + bs_2 Z_i - cs_2 Q_{i+1} - ds_2 Z_{i+1} \tag{A8}$$

where i and $i+1$ denote the locations of the cross-section; θ is Preissmann weighting coefficient; Q is the volumetric discharge; Z is the water level; L_t is the river width; t is time; V is the velocity; A is the flow area of cross section; $g = 9.81\ m\ s^{-2}$ is the gravitational acceleration; D is the conveyance function; P is wetted perimeter; R is hydraulic mean depth.

Appendix B. Constraint of probability non-negativity

Substitute coefficients in Appendix A into Eq. (3) and then Eq. (6), the transition probabilities can be written in the form as follow:

$$p = \frac{\frac{ds_2\theta + bs_1 cs_2}{cs_2 - as_2}}{\sum \frac{ds_1\theta + bs_1 cs_2}{cs_2 - as_2} + \frac{bs_2\theta - bs_1 as_2}{cs_2 - as_2}} \tag{B1}$$

or

$$p = \frac{\frac{bs_2\theta - bs_1 as_2}{cs_2 - as_1}}{\sum \frac{ds_2\theta + bs_1 cs_2}{cs_2 - as_1} + \frac{bs_2\theta - bs_1 as_2}{cs_2 - as_1}} \tag{B2}$$

Two assumptions are adopted here:

(a) Given the magnitude, the friction term is ignored in $cs_2 - as_1$. We can get $cs_2 - as_1 < 0$.

(b) Assuming $S_i \approx S_j$ and retaining the first term of the convection term, one has

$$bs_2\theta + bs_1 cs_2 \approx \frac{\theta^2}{2\Delta x}\left(D_i^2 + D_j^2\right)\left[\left(1 - Fr_i^2\right) + \frac{(\Delta x)^2}{\theta^2 2g h_j \Delta t}\left(-\frac{1}{2\Delta t} + \frac{2\theta}{\Delta x}V_j\right)\right] \tag{B3}$$

$$ds_2\theta - bs_1 as_2 \approx \frac{\theta^2}{2\Delta x}\left(D_i^2 + D_j^2\right)\left[\left(1 - Fr_j^2\right) + \frac{(\Delta x)^2}{\theta^2 2g h_i \Delta t}\left(-\frac{1}{2\Delta t} - \frac{2\theta}{\Delta x}V_i\right)\right] \tag{B4}$$

Probability non-negativity holds if Eq. (B3) and Eq. (B4) are the same as positive and negative signs. Considering the constraint of low Fr, these two equations should be all positive. That requires $\frac{(\Delta x)^2}{\theta^2 2g h \Delta t}\left(-\frac{1}{2\Delta t} \pm \frac{2\theta}{\Delta x}V\right) \geq Fr^2 - 1$.

References

Akan, A.O., Yen, B.C., 1981. Diffusion-wave flood routing in channel networks. J. Hydraul. Div. 107 https://doi.org/10.1061/JYCEAJ.0005681.

Akella, C.S., Bhallamudi, S.M., 2019. Managing municipal wastewater treatment to control nitrous oxide emissions from tidal rivers. Water (Switzerland) 11, 1–17. https://doi.org/10.3390/w11061255.

Assar, W., Ibrahim, M.G., Mahmod, W., Allam, A., Tawfik, A., Yoshimura, C., 2020. Effect of water shortage and pollution of irrigation water on water reuse for irrigation in the Nile Delta. J. Irrig. Drain. Eng. 146, 05019013. https://doi.org/10.1061/(ASCE)IR.1943-4774.0001439.

Bates, P.D., De Roo, A.P.J., 2000. A simple raster-based model for flood inundation simulation. J. Hydrol. 236, 54–77. https://doi.org/10.1016/S0022-1694(00)00278-X.

Beltaos, S., Tang, P., Rowsell, R., 2012. Ice jam modelling and field data collection for flood forecasting in the Saint John River, Canada. Hydrol. Process. 26, 2535–2545. https://doi.org/10.1002/hyp.9293.

Brunner, G.W., 2016. HEC-RAS, River Analysis System Hydraulic Reference Manual 5.0. U.S. Army Corps of Engineers' River Analysis System.

Brunner, G.W., 2018. HEC-RAS, River Analysis System Applications Guide 5.0.4. U.S. Army Corps of Engineers' River Analysis System.

Chen, dongyun, Tan, guangming, zheng, bangmin, 2001. Theory and practice of solving hydrodynamics equation with Monte-Carlo method. Adv. Sci. Technol. Water Resour. 2, 24–25 (in Chinese).

Choi, G.W., Molinas, A., 1993. Simultaneous solution algorithm for channel network modeling. Water Resour. Res. 29, 321–328. https://doi.org/10.1029/92WR01949.

Cunge, J.A., Holly, F.M., Verwey, A., 1980. Practical Aspects of Computational River Hydraulics. Pitman, London.

Dong, T.Y., Nittrouer, J.A., McElroy, B., Il'icheva, E., Pavlov, M., Ma, H., Moodie, A.J., Moreido, V.M., 2020. Predicting water and sediment partitioning in a delta channel network under varying discharge conditions. Water Resour. Res. 56, 1–21. https://doi.org/10.1029/2020WR027199.

El Kadi Abderrezzak, K., Paquier, A., 2009. One-dimensional numerical modeling of sediment transport and bed deformation in open channels. Water Resour. Res. 45, 1–20. https://doi.org/10.1029/2008WR007134.

Fang, H., Han, D., He, G., Chen, M., 2012. Flood management selections for the Yangtze River midstream after the three gorges project operation. J. Hydrol. 432–433, 1–11. https://doi.org/10.1016/j.jhydrol.2012.01.042.

Fovet, O., Litrico, X., Belaud, G., Genthon, O., 2013. Adaptive control of algae detachment in regulated canal networks. J. Hydroinf. 15, 321–334. https://doi.org/10.2166/hydro.2013.166.

Fread, D.L., 1973. Technique for implicit dynamic routing in rivers with tributaries. Water Resour. Res. 9, 918–926. https://doi.org/10.1029/WR009i004p00918.

Henine, H., Nédélec, Y., Ribstein, P., 2014. Coupled modelling of the effect of overpressure on water discharge in a tile drainage system. J. Hydrol. 511, 39–48. https://doi.org/10.1016/j.jhydrol.2013.12.016.

Hodges, B.R., 2019. Conservative finite-volume forms of the Saint-Venant equations for hydrology and urban drainage. Hydrol. Earth Syst. Sci. 23, 1281–1304. https://doi.org/10.5194/hess-23-1281-2019.

Janicke, L., Kost, A., 1998. Convergence properties of the Newton-Raphson method for nonlinear problems. IEEE Trans. Magn. 34, 2505–2508. https://doi.org/10.1109/20.717577.

Kesserwani, G., Ghostine, R., Vazquez, J., Ghenaim, A., Mosé, R., 2008a. Riemann solvers with Runge–Kutta discontinuous galerkin schemes for the 1D shallow water equations. J. Hydraul. Eng. 134, 243–255. https://doi.org/10.1061/(ASCE)0733-9429(2008)134:2(243).

Kesserwani, Georges, Ghostine, R., Vazquez, J., Mosé, R., Abdallah, M., Ghenaim, A., 2008b. Simulation of subcritical flow at open-channel junction. Adv. Water Resour. 31, 287–297. https://doi.org/10.1016/j.advwatres.2007.08.007.

LaBolle, E.M., Fogg, G.E., Tompson, A.F.B., 1996. Random-walk simulation of transport in heterogeneous porous media: local mass-conservation problem and implementation methods. Water Resour. Res. 32, 583–593. https://doi.org/10.1029/95WR03528.

Li, Q., Liang, Q., Xia, X., 2020. A novel 1D-2D coupled model for hydrodynamic simulation of flows in drainage networks. Adv. Water Resour. 137, 103519 https://doi.org/10.1016/j.advwatres.2020.103519.

Liang, D., Lin, B., Falconer, R.A., 2007. Simulation of rapidly varying flow using an efficient TVD–MacCormack scheme. Int. J. Numer. Methods Fluids 53, 811–826. https://doi.org/10.1002/fld.1305.

Liu, F., Hodges, B.R., 2014. Applying microprocessor analysis methods to river network modelling. Environ. Model. Softw. 52, 234–252. https://doi.org/10.1016/j.envsoft.2013.09.013.

Maire, S., Nguyen, G., 2016. Stochastic finite differences for elliptic diffusion equations in stratified domains. Math. Comput. Simul. 121, 146–165. https://doi.org/10.1016/j.matcom.2015.09.008.

Mascagni, M., Simonov, N.A., 2004. Monte Carlo methods for calculating some physical properties of large molecules. SIAM J. Sci. Comput. 26, 339–357. https://doi.org/10.1137/S1064827503422221.

Mazzoleni, M., Chacon-Hurtado, J., Noh, S.J., Seo, D.-J., Alfonso, L., Solomatine, D., 2018. Data assimilation in hydrologic routing: impact of model error and sensor placement on flood forecasting. J. Hydrol. Eng. 23, 1–15. https://doi.org/10.1061/(ASCE)HE.1943-5584.0001656.

Nan, T., Wu, J., 2018. Random walk path solution to groundwater flow dynamics in highly heterogeneous aquifers. J. Hydrol. 563, 543–559. https://doi.org/10.1016/j.jhydrol.2018.05.008.

Nan, T., Wu, J., Guadagnini, A., Zeng, X., Liang, X., 2020. Random walk evaluation of Green's functions for groundwater flow in heterogeneous aquifers. J. Hydrol. 588, 125029 https://doi.org/10.1016/j.jhydrol.2020.125029.

Nazari, B., Seo, D.J., 2021. Symbolic explicit solutions for 1-dimensional linear diffusive wave equation with lateral inflow and their applications. Water Resour. Res. 57 https://doi.org/10.1029/2019WR026906 e2019WR026906.

Nguyen, Q.K., Kawano, H., 1995. Simultaneous solution for flood routing in channel networks. J. Hydraul. Eng. 121, 744–750. https://doi.org/10.1061/(asce)0733-9429(1995)121:10(744).

Pappenberger, F., Matgen, P., Beven, K.J., Henry, J.B., Pfister, L., Fraipont, P., 2006. Influence of uncertain boundary conditions and model structure on flood inundation predictions. Adv. Water Resour. 29, 1430–1449. https://doi.org/10.1016/j.advwatres.2005.11.012.

Pu, J.H., Cheng, N.S., Tan, S.K., Shao, S., 2012. Source term treatment of SWEs using surface gradient upwind method. J. Hydraul. Res. 50, 145–153. https://doi.org/10.1080/00221686.2011.649838.

Qi, Y., Li, Q., Zhao, Z., Zhang, J., Gao, L., Yuan, W., Lu, Z., Nie, N., Shang, X., Tao, S., 2022. Heterogeneous parallel implementation of large-scale numerical simulation of saint-Venant equations. Appl. Sci. 12, 5671. https://doi.org/10.3390/app12115671.

Roubinet, D., Liu, H.-H., de Dreuzy, J.-R., 2010. A new particle-tracking approach to simulating transport in heterogeneous fractured porous media. Water Resour. Res. 46, 1–6. https://doi.org/10.1029/2010WR009371.

Sarkhosh, P., Salama, A., Jin, Y.C., 2020. A one-dimensional semi-implicit finite volume modeling of non-inertia wave through rockfill dams. J. Hydroinf. 22, 1485–1505. https://doi.org/10.2166/HYDRO.2020.056.

Sen, D.J., Garg, N.K., 1998. Efficient solution technique for dendritic channel networks using FEM. J. Hydraul. Eng. 124, 831–839. https://doi.org/10.1061/(ASCE)0733-9429(1998)124:8(831).

Sen, D.J., Garg, N.K., 2002. Efficient algorithm for gradually varied flows in channel networks. J. Irrig. Drain. Eng. 128, 351–357. https://doi.org/10.1061/(ASCE)0733-9437(2002)128:6(351).

Simonov, N.A., Mascagni, M., 2004. Random walk algorithms for estimating effective properties of digitized porous media *. Monte Carlo Methods Appl. 10, 599–608. https://doi.org/10.1515/mcma.2004.10.3-4.599.

Tang, H., Cao, H., Yuan, S., Xiao, Y., Jiang, C., Gualtieri, C., 2020. A numerical study of hydrodynamic processes and flood mitigation in a large river-lake system. Water Resour. Manag. 34, 3739–3760. https://doi.org/10.1007/s11269-020-02628-y.

Tian, X., Guo, Y., Negenborn, R.R., Wei, L., Lin, N.M., Maestre, J.M., 2019. Multi-scenario model predictive control based on genetic algorithms for level regulation of open water systems under ensemble forecasts. Water Resour. Manag. 33, 3025–3040. https://doi.org/10.1007/s11269-019-02284-x.

Wang, Jiabiao, Lei, Xiaohui, Liao, Weihong, Wang, Hao, 2016. Study on application of random walk method in looping river network computation. Syst. Eng. Theory Pract. 36 (8), 2169–2176. https://doi.org/10.12011/1000-6788(2016)08-2169-08.

Xu, M., van Overloop, P.J., van de Giesen, N.C., 2011. On the study of control effectiveness and computational efficiency of reduced saint-Venant model in model predictive control of open channel flow. Adv. Water Resour. 34, 282–290. https://doi.org/10.1016/j.advwatres.2010.11.009.

Yang, F., Liang, D., 2020. Random-walk simulation of non-conservative pollutant transport in shallow water flows. Environ. Model. Softw. 134, 104870 https://doi.org/10.1016/j.envsoft.2020.104870.

Yuan, S., Tang, H., Li, K., Xu, L., Xiao, Y., Gualtieri, C., Rennie, C., Melville, B., 2021. Hydrodynamics, sediment transport and morphological features at the confluence between the Yangtze River and the Poyang Lake. Water Resour. Res. 57, 1–24. https://doi.org/10.1029/2020WR028284.

Yuan, S., Xu, Yu, Tang, L., Wu, H., Xiao, Y., Gualtieri, C., 2022. The dynamics of river confluences and their effects on the ecology of aquatic environment: a review. J. Hydrodyn. 34, 1–14. https://doi.org/10.1007/s42241-022-0001-z.

Zhang, M., Shen, Y., 2007. Mathematical model for channel networks. J. Hydrodyn. 19, 572–578.

Zhao, J., Özgen-Xian, I., Liang, D., Wang, T., Hinkelmann, R., 2019. An improved multislope MUSCL scheme for solving shallow water equations on unstructured grids. Comput. Math. Appl. 77, 576–596. https://doi.org/10.1016/j.camwa.2018.09.059.

Zhu, D., Chen, Y., 2019. Implementing of the JPWSPC method in RIV1H for unsteady flow modeling in general river networks. Int. J. Sed. Res. 34, 379–386. https://doi.org/10.1016/j.ijsrc.2018.12.003.

Zhu, D., Chen, Y., Wang, Z., Liu, Z., 2011. Simple, robust, and efficient algorithm for gradually varied subcritical flow simulation in general channel networks. J. Hydraul. Eng. 137, 766–774. https://doi.org/10.1061/(asce)hy.1943-7900.0000356.